

Linear Flavor-Wave Analysis of SU(4)-Symmetric Tetramer Model with Population Imbalance

Yuki Miyazaki^{1*}, Giacomo Marmorini^{1,2}, Nobuo Furukawa¹, and Daisuke Yamamoto²

¹*Department of Physics and Mathematics, Aoyama Gakuin University, Sagami-hara, Kanagawa 252-5258, Japan*

²*Department of Physics, College of Humanities and Sciences, Nihon University, Sakurajosui, Setagaya, Tokyo 156-8550, Japan*

We study the quantum magnetism of the SU(4) Mott insulator in a square optical superlattice, in which atoms with four nuclear-spin components strongly interact with each other, in the presence of an external field that controls the imbalance between the population of two components and that of the other two. This is a natural extension of the physics of spin-dimer materials under strong magnetic field. We apply an extended linear flavor-wave theory based on four-site plaquettes and unveil the ground-state phase diagram and excitation spectra. When the population of the four components is balanced and the plaquettes are weakly coupled, the ground state is approximately given by the direct product of local SU(4)-singlet states. In high-field, the system reaches a “saturated state” where only two components are present. Our main finding is a nontrivial intermediate phase, which has a checkerboard-like arrangement of the SU(4)-singlet and four-site resonating-valence-bond states.

Quantum dimer magnets, which consist of a weakly coupled network of $S = 1/2$ spin pairs, have been attracting attention as a prototypical example for studying novel phases of matter and quantum phase transitions. Spin-dimer materials such as TiCuCl_3 ^{1–3)} feature a non-magnetic gapped ground state, which is continuously connected to a direct product of spin-singlet states. The lowest excitations to one of the spin-triplet states behave like bosonic quasiparticles, called triplons. When a magnetic field is applied, the energy gap decreases and eventually closes at a certain critical field. The resulting quantum phase transition from non-magnetic to magnetic state can be explained by Bose-Einstein condensation of triplons. Some exceptional spin-dimer materials with strong frustration effects, *e.g.*, $\text{Ba}_2\text{CoSi}_2\text{O}_6\text{Cl}_2$,⁴⁾ which exhibits a crystallized state of localized triplons, and $\text{SrCu}_2(\text{BO}_3)_2$,⁵⁾ characterized by orthogonal dimers forming a Shastry-Sutherland lattice, have also been studied with great interest.

In the field of cold atomic and optical physics, a great deal of effort is being made to explore exotic quantum magnetism using ultracold atomic gases loaded in an optical lattice.^{6–8)} One of the recent remarkable achievements is the observation of long-range antiferromagnetic correlations of an artificial antiferromagnet realized with the two lowest hyperfine states of the fermionic species ^6Li .⁹⁾ Besides the conventional SU(2) systems, there has been success in realizing higher symmetric Mott insulators with alkaline-earth(-like) atoms such as ^{173}Yb .^{10,11)} Those atoms are closed-shell in the ground state, and the nuclear spin provides $2I + 1$ states (flavors), where $I = 5/2$ for ^{173}Yb . With these atomic species one can prepare ideal SU($\mathcal{N} > 2$)-symmetric systems because the interatomic interaction does not depend on the nuclear spin to a great approximation.¹²⁾ Quantum magnetism

with a high SU(\mathcal{N}) symmetry has great potential to feature exotic phase transition phenomena associated with a rich variety of spontaneous symmetry breaking.

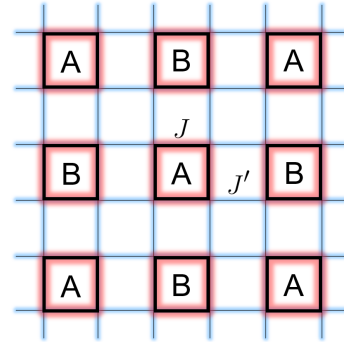


Fig. 1. Sketch of the tetramerized square lattice with the assumed two-sublattice structure. The line thickness represents the strength of the interactions; $J \gg J' > 0$.

Here, we consider the square superlattice in which the lattice sites are tetramerized as shown in Fig. 1 and focus on the case where each of the sites is singly occupied by one of four pseudospin components (flavors) of fermions with the SU(4) symmetry. To study the strong coupling physics, we describe the system by an extended antiferromagnetic Heisenberg model with each site comprising the fundamental representation of the SU(4) group.

In cold-atom experiments, such an optical superlattice can be created by superimposing long-period and short-period optical square lattices.¹³⁾ Progress in loading the above-mentioned ytterbium isotope in this kind of superlattice has already been reported.¹⁶⁾ In the field of conventional SU(2) magnetism, analogous plaquette-based

*y-miyazaki@phys.aoyama.ac.jp

models have been considered.^{14,15)} Let us also mention that SU(4) symmetry has seen a recent revival in models of spin-orbital physics in solid state compounds, *e.g.* α -ZrCl₃.¹⁷⁾

Hereafter, let us name the four flavors “u”, “d”, “c”, and “s” after the quark model. The SU(4) Heisenberg model with a multiplet in the fundamental representation at each site is given by the Hamiltonian^{18,19,32,37)}

$$\hat{\mathcal{H}}_{\text{SU}(4)} = \sum_{\langle i,j \rangle} \sum_{\mu,\nu} J_{i,j} \hat{F}_\mu^\nu(i) \hat{F}_\nu^\mu(j) \quad (1)$$

where $J_{i,j}$ are superexchange couplings; they take the value $J(>0)$ within a plaquette and $J'(>0)$ between neighboring plaquettes. We define the flavor-changing operator $\hat{F}_\mu^\nu(i) \equiv |\mu(i)\rangle\langle\nu(i)|$, where $\mu, \nu \in \{u, d, c, s\}$. For an isolated plaquette ($J' = 0$), there are five energy levels: the lowest one is non-degenerate and corresponds to the SU(4) singlet state, namely the fully antisymmetrized state $\frac{1}{\sqrt{24}} \sum_{\{i,j,k,l\}} \hat{c}_{iu}^\dagger \hat{c}_{jd}^\dagger \hat{c}_{kc}^\dagger \hat{c}_{ls}^\dagger |\text{vac}\rangle$, where $\sum_{\{i,j,k,l\}}$ denotes the summation over the 24 possible permutations of site indexes i, j, k , and l and $\hat{c}_{i\mu}^\dagger$ is the creation operator of a fermion at site i with flavor μ .²⁰⁾ Each of the other four levels is massively degenerate. In order to consider a natural extension of the spin-dimer physics to SU(4), we apply an external field which controls the population imbalance between $\{u, d\}$ and $\{c, s\}$ and study the Hamiltonian $\hat{\mathcal{H}} = \hat{\mathcal{H}}_{\text{SU}(4)} + \hat{\mathcal{H}}_D$, where

$$\hat{\mathcal{H}}_D = D \sum_i \left[\hat{F}_c^\dagger(i) + \hat{F}_s^\dagger(i) - \hat{F}_u^\dagger(i) - \hat{F}_d^\dagger(i) \right]. \quad (2)$$

When the value of $D(>0)$ is increased, the population of $\{u, d\}$ tends to increase while $\{c, s\}$ components are disfavored. This presents as a natural analogy with the conventional magnetic field for SU(2) spins in terms of dividing the single-particle energy levels into two levels symmetrically. For the case of isolated tetramers ($J' = 0$), the transition from the SU(4)-singlet state to the four-site resonating-valence-bond state of u and d (RVB_{ud}) occurs via the energy level crossing at $D/J = 1/2$ as shown in Fig. 2. In previous works, the four-site RVB state was created using two atomic states of ⁸⁷Rb loaded into a plaquette of an optical lattice, and observed by the singlet-triplet oscillation technique^{24,25)}. For finite $J'(>0)$, the appearance of a nontrivial intermediate phase between SU(4) singlet phase and RVB_{ud} phase is expected, in analogy with spin dimer magnets.

We study the ground state of the Hamiltonian $\hat{\mathcal{H}}$ using an extended linear flavor-wave theory (LFWT)^{29–34)} based on four-site plaquettes. First, we reduce the full problem to a four-site one by applying the mean-field approximation $\hat{F}_\mu^\nu(i) \hat{F}_\nu^\mu(j) \approx \langle \hat{F}_\mu^\nu(i) \rangle \hat{F}_\nu^\mu(j) + \langle \hat{F}_\nu^\mu(j) \rangle \hat{F}_\mu^\nu(i) - \langle \hat{F}_\mu^\nu(i) \rangle \langle \hat{F}_\nu^\mu(j) \rangle$ to the interplaquette bonds; this approach, named plaquette mean-field (PMF) method, is clearly justified for small J' . We calculate the mean-field parameters $\{\langle \hat{F}_\mu^\nu(i) \rangle\}$ self-consistently via the solution of the four-site problem under the assumption of the plaquette-checkerboard pattern shown in Fig. 1.^{21–23)} Subsequently, we include the interplaquette quantum correlation around the PMF

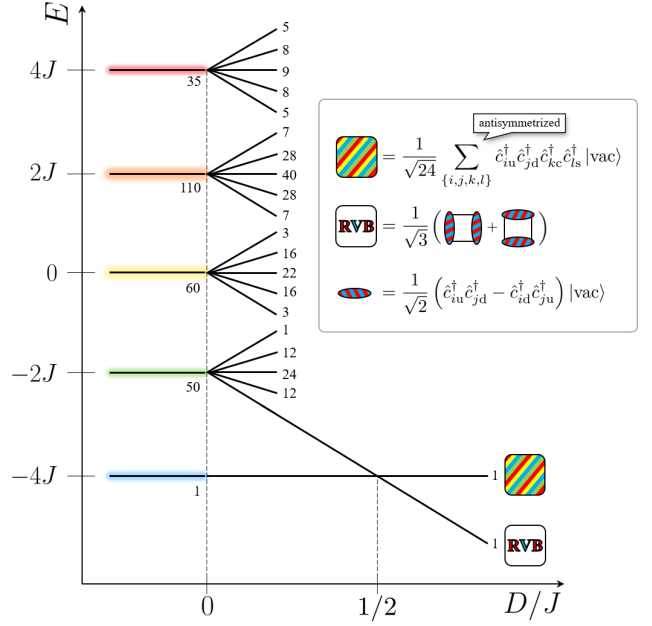


Fig. 2. The energy levels of an isolated plaquette described by the SU(4) Heisenberg model under an external field that controls the population imbalance between two components and the other two. The numbers attached to each level are the degree of degeneracy.

ground state. To this end, we rewrite the Hamiltonian $\hat{\mathcal{H}}$ in terms of the creation (and annihilation) operators of the ground and excited states of the PMF Hamiltonian, \hat{g}_I^\dagger and $\{\hat{e}_{I,n}^\dagger\}$, where I denotes the plaquette index and n labels the 255 excited states. Those operators obey the bosonic commutation relations under the constraint

$$\hat{g}_I^\dagger \hat{g}_I + \sum_n \hat{e}_{I,n}^\dagger \hat{e}_{I,n} = 1. \quad (3)$$

Following the analogy with the spin-wave method,^{26–28)} we may expand the Hamiltonian with

$$\hat{g}_I^\dagger = \sqrt{1 - \sum_n \hat{e}_{I,n}^\dagger \hat{e}_{I,n}} \simeq 1 - \frac{1}{2} \sum_n \hat{e}_{I,n}^\dagger \hat{e}_{I,n} + \dots, \quad (4)$$

under the assumption that the fluctuations $\sum_n \hat{e}_{I,n}^\dagger \hat{e}_{I,n}$ around the PMF ground state are sufficiently small; this can be verified *a posteriori* in a large region of the parameter space (see the Supplementary Material⁴⁵⁾). The Hamiltonian becomes

$$\hat{\mathcal{H}} = E_0 + \hat{\mathcal{H}}_1 + \hat{\mathcal{H}}_2 + \hat{\mathcal{H}}_3 + \dots, \quad (5)$$

where E_0 is the energy within the PMF approximation and $\hat{\mathcal{H}}_n$ denotes the n -th order correction in $\hat{e}_{I,n}^\dagger, \hat{e}_{I,n}$. Note that $\hat{\mathcal{H}}_1 = 0$ is satisfied. Performing the Fourier transformation ($\hat{e}_{I,n} \rightarrow \hat{e}_{\mathbf{k},n}$) and the diagonalization via the generalized Bogoliubov transformation ($\hat{e}_{\mathbf{k},n} \rightarrow \hat{\epsilon}_{\mathbf{k},\lambda}$),³⁵⁾ we obtain

$$\hat{\mathcal{H}}_2 = \sum_{\mathbf{k}} \sum_{\lambda=1}^{510} \omega_{\mathbf{k},\lambda} \hat{\epsilon}_{\mathbf{k},\lambda}^\dagger \hat{\epsilon}_{\mathbf{k},\lambda} + E_{\text{zp}}, \quad (6)$$

where $\omega_{\mathbf{k},\lambda}$ is the λ -th excitation energy band and

$$E_{\text{zp}} = \frac{1}{2} \sum_{\mathbf{k}} \sum_{\lambda} \omega_{\mathbf{k},\lambda} - \frac{1}{2} \sum_{\mathbf{k}} \text{Tr} A_{-\mathbf{k}}^*. \quad (7)$$

is the zero-point energy. Here, $A_{-\mathbf{k}}^*$ is the bottom-right 510×510 block of the Bogoliubov matrix representation of $\hat{\mathcal{H}}_2$.^{35,36)} See the Supplementary Material⁴⁵⁾ for more technical details.

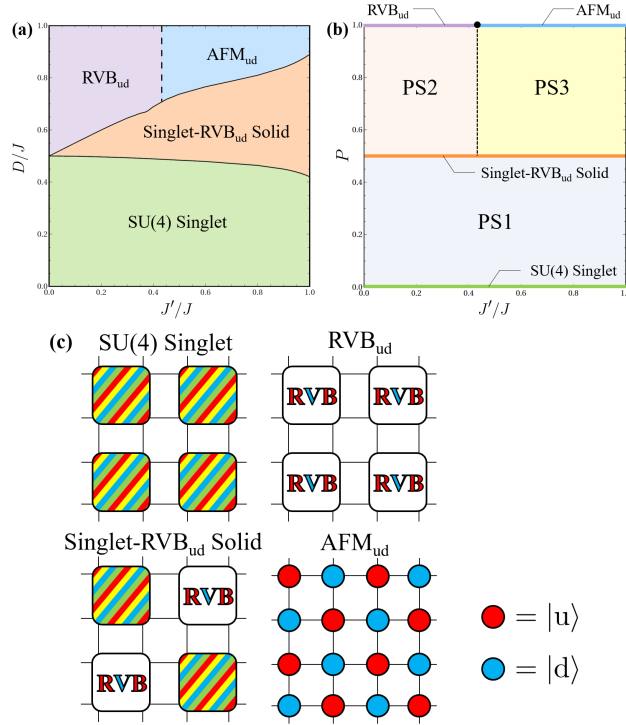


Fig. 3. (a) Ground-state phase diagram in the J'/J vs. D/J plane within LFWT. Dashed and solid lines represent second-order and first-order boundaries, respectively. (b) The phase diagram in the J'/J vs. P plane. (c) Sketches of each phase (see also Fig. 2).

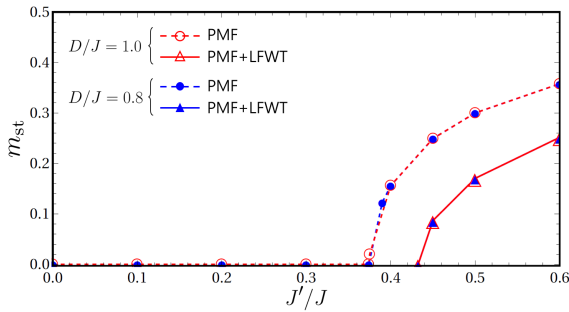


Fig. 4. The staggered magnetization for increasing J'/J at $D/J = 0.8$ and $D/J = 1.0$ calculated by PMF (circles) and PMF+LFWT (triangles).

Figure 3(a) shows the ground-state phase diagram in the plane of J'/J vs. D/J within the PMF+LFWT cal-

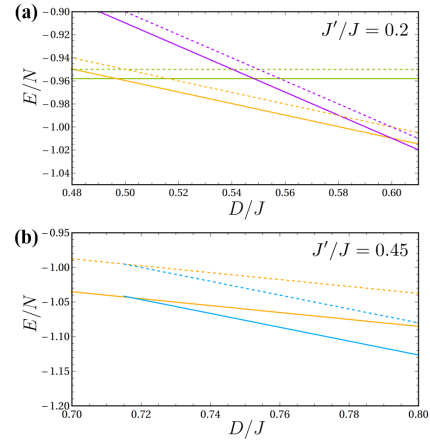


Fig. 5. The energy per site as a function of D/J at (a) $J'/J = 0.2$ and (b) $J'/J = 0.45$. The color code is as follows: green for SU(4) singlet, orange for SU(4)-RVB_{ud} solid, violet for RVB_{ud}, and light blue for AFM_{ud}. The dashed and solid lines represent E_0/N and $(E_0 + E_{\text{zp}})/N$, respectively.

culations. We also show the phase diagram in the plane of J'/J vs. P [Fig. 3(b)], where $P \equiv -\langle \partial \hat{\mathcal{H}} / \partial D \rangle / N$ is the conjugate variable of D . In the regions labeled PS1, PS2, and PS3, phase separation of the two phases which sandwich the respective PS region occurs: SU(4) singlet and singlet-RVB_{ud} solid phases for PS1, singlet-RVB_{ud} solid and RVB_{ud} phases for PS2, and singlet-RVB_{ud} solid and AFM_{ud} phases for PS3. The phase domains differ by the value of P , that can be rewritten as

$$P = \frac{\langle \hat{N}_u \rangle + \langle \hat{N}_d \rangle - \langle \hat{N}_c \rangle - \langle \hat{N}_s \rangle}{N}, \quad (8)$$

where $\hat{N}_\mu = \sum_i \hat{c}_{i\mu}^\dagger \hat{c}_{i\mu} = \sum_i \hat{F}_\mu^\mu(i)$ is the total number operator of particles of flavor μ . The sketches of each phase are depicted in Fig. 3(c). Note that our LFWT analysis, being based on the PMF approximation, can reliably describe the physics at relatively small values of J'/J .

In the SU(4) singlet phase, since the population of the four components is balanced, the value of P is zero. In the RVB_{ud} phase, instead, $P = 1$ because both c and s components are absent. In fact, when the value of D is large enough the system can be mapped to a simple SU(2)-symmetric system with only u and d components. When the value of J' is increased in such a regime, a second-order phase transition from RVB_{ud} to Néel anti-ferromagnetic phase of u and d (AFM_{ud}) occurs, whose characteristic order parameter is the staggered magnetization. In order to determine the critical point, we consider the Hamiltonian with staggered magnetic field:

$$\hat{\mathcal{H}} = \hat{\mathcal{H}}_{\text{SU}(4)} + \hat{\mathcal{H}}_D - h_{\text{st}} \sum_i (-1)^i \hat{S}_i^z, \quad (9)$$

where

$$\hat{S}_i^z = \frac{1}{2} \hat{F}_u^u(i) - \frac{1}{2} \hat{F}_d^d(i) + \frac{3}{2} \hat{F}_c^c(i) - \frac{3}{2} \hat{F}_s^s(i). \quad (10)$$

The PMF staggered magnetization m_{st} and the LFWT

correction δm_{st} are given by the thermodynamic relation:

$$m_{\text{st}} + \delta m_{\text{st}} = -\frac{1}{N} \left. \frac{d(E_0 + E_{\text{zp}})}{dh_{\text{st}}} \right|_{h_{\text{st}}=0}. \quad (11)$$

The critical line, signaled by the onset of the staggered magnetization, is $(J'/J)_c \simeq 0.374$ at the PMF level and 0.432 within PMF+LFWT, independently of D , as shown in Fig. 4. In terms of P , the AFM_{ud} phase is also characterized by $P = 1$. RVB_{ud} phase and AFM_{ud} phase are divided by the critical point $(J'/J)_c$ [Fig. 3(b)]. The most interesting feature of the phase diagram is a nontrivial intermediate phase between SU(4) singlet and RVB_{ud} phases. It is the checkerboard configuration of SU(4)-singlet and RVB_{ud} plaquettes, which we name “singlet-RVB_{ud} solid”. Since the number of $\{u, d\}$ is twice that of $\{c, s\}$, this phase is characterized by $P = 1/2$. The various first-order phase transitions from this phase to the others are due to the energy level crossings depicted in Fig. 5.

Figures 6(a)-(f) show the low-energy excitations for various choices of parameters within PMF+LFWT. At the critical point $(J'/J)_c \simeq 0.374$, there appears a Nambu-Goldstone mode in the LFWT spectrum $\omega_{\mathbf{k}}$, which is gapless at the Γ point [Fig. 6(c)]. This is because of the spontaneous symmetry breaking of SU(2) down to U(1) in AFM_{ud} phase [Fig. 6(f)]. At the PMF phase boundaries between SU(4) singlet and singlet-RVB_{ud} solid phases and between singlet-RVB_{ud} solid and AFM_{ud} phases, there appears a lowest-energy flat band responsible for the gap closing at all wave-vectors \mathbf{k} [Fig. 6(a), (b), (d), and (e)]. This arises from the infinite degeneracy of the ground state at the PMF level. However, this will be changed with the inclusion of corrections beyond LFWT, that will give these bands a finite width.

Lastly, let us comment about previous works on the SU(4) Heisenberg model on a uniform square lattice ($D/J = 0$, $J'/J = 1$ in our model), where it is suggested that the ground state is the dimer Néel phase.³⁷⁾ In our study, we cannot confirm the stability of the dimer Néel phase at any point in the phase diagram; however, we ascribe this to the limitations of the PMF+LFWT method, which gives reasonable results at relatively small J'/J but is not suitable for the uniform lattice limit.

In conclusion, we investigate a natural extension of the spin-dimer materials to SU(4)-symmetric tetramer systems and study the quantum phase transitions in the presence of flavor population imbalance using the PMF+LFWT. We unveil the ground-state phase diagram and show the low-energy excitation spectrum. We find a nontrivial intermediate phase in the saturation process of the order parameter Eq. 8. The Hamiltonian we discussed can be realized by loading ^{173}Yb atoms, whose nuclear spin state populations can be controlled by the optical pumping technique,³⁸⁾ into an optical superlattice.¹³⁾ One way to neatly detect the new intermediate phase is to observe atoms on each site directly by quantum-gas microscope;^{9, 39–44)} this kind of measurement is, however, still not easy in SU(\mathcal{N}) cold atom experiments. On the other hand, probing the system with the singlet-triplet oscillation technique, already success-

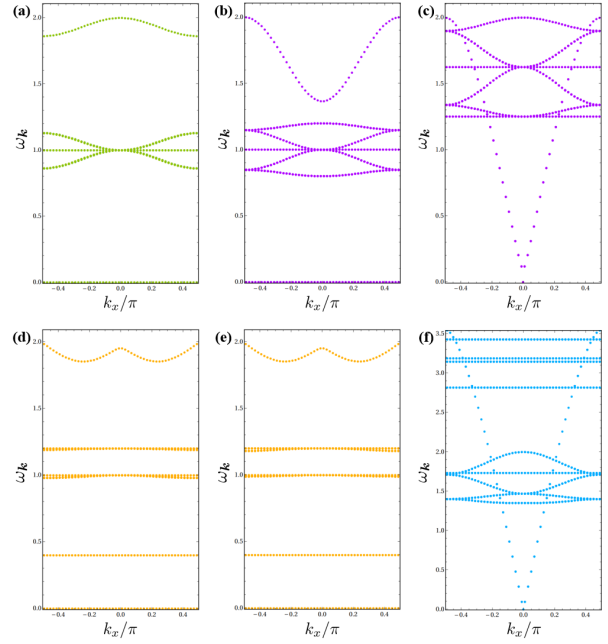


Fig. 6. Low-lying excitation spectra calculated from (a) SU(4) singlet phase at $J'/J = 0.2$, $D/J = 0.5$, (b) RVB_{ud} phase at $J'/J = 0.2$, $D/J = 0.6$ and (c) $J'/J = 0.374$, $D/J = 1.0$, (d) Singlet-RVB_{ud} solid phase at $J'/J = 0.2$, $D/J = 0.5$ and (e) $D/J = 0.6$, and (f) AFM_{ud} phase at $J'/J = 1.0$, $D/J = 1.0$. Now the first Brillouin zone is a square with vertices $(-\pi/2, 0)$, $(0, -\pi/2)$, $(\pi/2, 0)$, and $(0, \pi/2)$, but here we show the plots along the k_x axis.

fully used in SU(\mathcal{N}) experiments,³⁸⁾ could provide a significant, if indirect, signal.

We thank Y. Takahashi, Y. Takasu, and S. Taie, I. Danshita, and S. Tsuchiya for useful discussions. This work was supported by JSPS KAKENHI Grant Nos. 18K03525 and 21H05185 (D.Y.) and JST PRESTO Grant No. JPMJPR2118, Japan (D.Y.).

- 1) T. Nikuni, M. Oshikawa, A. Oosawa, and H. Tanaka, *Physical Review Letters* **84**, 5868 (2000).
- 2) F. Yamada, T. Ono, H. Tanaka, G. Misguich, M. Oshikawa, and T. Sakakibara, *Journal of the Physical Society of Japan* **77**, 013701 (2007).
- 3) M. Matsumoto, B. Normand, T. M. Rice, and M. Sigrist, *Physical Review B* **69**, 054423 (2004).
- 4) N. Kurita, D. Yamamoto, T. Kanesaka, N. Furukawa, S. Ohira-Kawamura, K. Nakajima, and H. Tanaka, *Physical Review Letters* **123**, 027206 (2019).
- 5) A. Koga and N. Kawakami, *Physical Review Letters* **84**, 4461 (2000).
- 6) G. Pagano, M. Mancini, G. Cappellini, P. Lombardi, F. Schäfer, H. Hu, X.-J. Liu, J. Catani, C. Sias, M. Inguscio, and L. Fallani, *Nature Physics* **10**, 198 (2014).
- 7) F. Scazza, C. Hofrichter, M. Höfer, P. C. De Groot, I. Bloch, and S. Fölling, *Nature Physics* **10**, 779 (2014).
- 8) X. Zhang, M. Bishof, S. L. Bromley, C. V. Kraus, M. S. Safronova, P. Zoller, A. M. Rey, and J. Ye, *Science* **345**, 1467 (2014).
- 9) A. Mazurenko, C. S. Chiu, G. Ji, M. F. Parsons, M. Kanász-Nagy, R. Schmidt, F. Grusdt, E. Demler, D. Greif, and M. Greiner, *Nature* **545**, 462 (2017).
- 10) S. Taie, R. Yamazaki, S. Sugawa, and Y. Takahashi, *Nature Physics* **8**, 825 (2012).

-
- 11) C. Hofrichter, L. Riegger, F. Scazza, M. Höfer, D. R. Fernandes, I. Bloch, and S. Fölling, *Physical Review X* **6**, 021030 (2016).
 - 12) S. Taie, Y. Takasu, S. Sugawa, R. Yamazaki, T. Tsujimoto, R. Murakami, and Y. Takahashi, *Physical Review Letters* **105**, 190401 (2010).
 - 13) S. Fölling, S. Trotzky, P. Cheinet, M. Feld, R. Saers, A. Widera, T. Müller, and I. Bloch, *Nature* **448**, 1029 (2007).
 - 14) M.E. Zhitomirsky and K. Ueda, *Physical Review B* **54**, 9007 (1996).
 - 15) H.T. Ueda and K. Totsuka, *Physical Review B* **76**, 214428 (2007).
 - 16) Y. Takahashi, Talk at 51st Annual Meeting of the APS Division of Atomic, Molecular and Optical Physics, June 2020.
 - 17) M. G. Yamada, M. Oshikawa, and G. Jackeli, *Phys. Rev. Lett.* **121**, 097201 (2018).
 - 18) P. Nataf and F. Mila, *Physical Review Letters* **113**, 127204 (2014).
 - 19) P. Nataf, M. Lajkó, P. Corboz, A. M. Läuchli, K. Penc, and F. Mila, *Physical Review B* **93**, 201113(R) (2016).
 - 20) Y.-Q. Li, M. Ma, D. Shi, and F. Zhang, *Physical Review Letters* **81**, 3527 (1998).
 - 21) D. Yamamoto, A. Masaki, and I. Danshita, *Physical Review B* **86**, 054516 (2012).
 - 22) D. Yamamoto, G. Marmorini, and I. Danshita, *Physical Review Letters* **112**, 127203 (2014).
 - 23) D. Yamamoto, C. Suzuki, G. Marmorini, S. Okazaki, and N. Furukawa, *Physical Review Letters* **125**, 057204 (2020).
 - 24) B. Paredes and I. Bloch, *Physical Review A* **77**, 023603 (2008).
 - 25) S. Nascimbène, Y.-A. Chen, M. Atala, M. Aidelsburger, S. Trotzky, B. Paredes, and I. Bloch, *Physical Review Letters* **108**, 205301 (2012).
 - 26) P. W. Anderson, *Physical Review*, **86**, 694 (1952).
 - 27) E. Manousakis, *Reviews of Modern Physics*, **63**, 1 (1991).
 - 28) M. E. Zhitomirsky and T. Nikuni, *Physical Review B* **57**, 5013 (1998).
 - 29) N.Papanicolaou, *Nuclear Physics B* **240**, 281 (1984).
 - 30) N.Papanicolaou, *Nuclear Physics B* **305**, 367 (1988).
 - 31) A. Joshi, M. Ma, F. Mila, D. N. Shi, and F. C. Zhang, *Physical Review B* **60**, 6584 (1999).
 - 32) T. A. Tóth, A. M. Läuchli, F. Mila, and K. Penc, *Physical Review Letters* **105**, 265301 (2010).
 - 33) B. Bauer, P. Corboz, A. M. Läuchli, L. Messio, K. Penc, M. Troyer, and F. Mila., *Physical Review B*, **85**, 125116 (2012).
 - 34) F. H. Kim, K. Penc, P. Nataf, and F. Mila, *Physical Review B* **96**, 205142 (2017).
 - 35) J. H. P. Colpa, *Physica A* **134**, 377 (1986).
 - 36) R. Shindou, R. Matsumoto, S. Murakami, and J. Ohe, *Physical Review B* **87**, 174427 (2013).
 - 37) P. Corboz, A. M. Läuchli, K. Penc, M. Troyer, and F. Mila, *Physical Review Letters* **107**, 215301 (2011).
 - 38) H. Ozawa, S. Taie, Y. Takasu, and Y. Takahashi, *Physical Review Letters* **121**, 225303 (2018).
 - 39) W. S. Bakr, J. I. Gillen, A. Peng, S. Fölling, and M. Greiner, *Nature* **462**, 74 (2009).
 - 40) L. W. Cheuk, M. A. Nichols, M. Okan, T. Gersdorf, V. V. Ramasesh, W. S. Bakr, T. Lompe, and M. W. Zwierlein, *Physical Review Letters* **114**, 193001 (2015).
 - 41) E. Haller, J. Hudson, A. Kelly, D. A. Cotta, B. Peaudecerf, G. D. Bruce, and S. Kuhr, *Nature Physics* **11**, 738 (2015).
 - 42) M. Miranda, R. Inoue, Y. Okuyama, A. Nakamoto, and M. Kozuma, *Physical Review A* **91**, 063414 (2015).
 - 43) R. Yamamoto, J. Kobayashi, T. Kuno, K. Kato, and Y. Takahashi, *New Journal of Physics* **18** 023016 (2016).
 - 44) M. Miranda, R. Inoue, N. Tambo, and M. Kozuma, *Physical Review A* **96**, 043626 (2017).
 - 45) Supplementary material.

Supplementary Material for “Linear Flavor-Wave Analysis of SU(4)-Symmetric Tetramer Model with Population Imbalance”

Yuki Miyazaki^{1*}, Giacomo Marmorini^{1,2}, Nobuo Furukawa¹, and Daisuke Yamamoto²

¹*Department of Physics and Mathematics, Aoyama Gakuin University, Sagamihara,
Kanagawa 252-5258, Japan*

²*Department of Physics, College of Humanities and Sciences, Nihon University,
Sakurajosui, Setagaya, Tokyo 156-8550, Japan*

1. PLAQUETTE MEAN-FIELD APPROXIMATION

Let us rewrite the Hamiltonian $\hat{\mathcal{H}} = \hat{\mathcal{H}}_{\text{SU}(4)} + \hat{\mathcal{H}}_D$ in the main text as follows:

$$\begin{aligned} \hat{\mathcal{H}} = & J \sum_I \sum_{\langle n, n' \rangle} \sum_{\mu, \nu} \hat{F}_\mu^\nu(I_n) \hat{F}_\nu^\mu(I_{n'}) + \sum_I \sum_{I'} \sum_{n, n'=1}^{N/4} \sum_{\mu, \nu} \mathcal{J}'_{I_n, I'_{n'}} \hat{F}_\mu^\nu(I_n) \hat{F}_\nu^\mu(I'_{n'}) \\ & + D \sum_I \sum_{n=1}^4 \left[\hat{F}_c^\nu(I_n) + \hat{F}_s^\nu(I_n) - \hat{F}_u^\nu(I_n) - \hat{F}_d^\nu(I_n) \right]. \end{aligned} \quad (\text{S1})$$

N is the total number of sites and I_n denotes a site in plaquette I : I_1 for the top-left, I_2 for the top-right, I_3 for the bottom-right, and I_4 for the bottom-left (clock-wise convention). $\langle n, n' \rangle$ denotes the pairs of neighboring sites in a plaquette. We define

$$\mathcal{J}'_{I_n, I'_{n'}} = \begin{cases} J' & \text{if } |\mathbf{r}_{I'_{n'}} - \mathbf{r}_{I_n}| = 1 \text{ and } I \neq I' \\ 0 & \text{otherwise} \end{cases}. \quad (\text{S2})$$

In order to reduce the full problem on the tetramerized square lattice shown in Fig. 1 to a four-site one, we apply the mean-field approximation $\hat{F}_\mu^\nu(I_n) \hat{F}_\nu^\mu(I'_{n'}) \approx \langle \hat{F}_\mu^\nu(I_n) \rangle \hat{F}_\nu^\mu(I'_{n'}) + \langle \hat{F}_\nu^\mu(I'_{n'}) \rangle \hat{F}_\mu^\nu(I_n) - \langle \hat{F}_\mu^\nu(I_n) \rangle \langle \hat{F}_\nu^\mu(I'_{n'}) \rangle$ to the interplaquette bonds. We obtain the following plaquette mean-field (PMF) Hamiltonian:

$$\hat{\mathcal{H}}_I^{\text{PMF}} = \sum_{\langle n, n' \rangle} \sum_{\mu, \nu} \hat{F}_\mu^\nu(I_n) \hat{F}_\nu^\mu(I_{n'})$$

*y-miyazaki@phys.aoyama.ac.jp

$$\begin{aligned}
& + \sum_{I'}^{N/4} \sum_{n,n'=1}^4 \sum_{\mu,\nu} \mathcal{J}'_{I_n, I'_{n'}} \left[\hat{F}_\mu^\nu(I_n) \langle \hat{F}_\nu^\mu(I'_{n'}) \rangle + \hat{F}_\nu^\mu(I'_{n'}) \langle \hat{F}_\mu^\nu(I_n) \rangle - \langle \hat{F}_\mu^\nu(I_n) \rangle \langle \hat{F}_\nu^\mu(I'_{n'}) \rangle \right] \\
& + D \sum_{n=1}^4 \left[\hat{F}_c^c(I_n) + \hat{F}_s^s(I_n) - \hat{F}_u^u(I_n) - \hat{F}_d^d(I_n) \right]. \tag{S3}
\end{aligned}$$

Under the assumption of the plaquette-checkerboard pattern of the mean-field parameters shown in Fig. 1, we rewrite $\hat{\mathcal{H}}$ as $\hat{\mathcal{H}} = \sum_{I \in A} \hat{\mathcal{H}}_I^{\text{PMF}} + \sum_{I \in B} \hat{\mathcal{H}}_I^{\text{PMF}}$. At this stage we are thus neglecting the interplaquette quantum entanglement. We self-consistently calculate the mean-field parameters $\{\langle \hat{F}_\mu^\nu(I_n \in A) \rangle\}$ and $\{\langle \hat{F}_\mu^\nu(I_n \in B) \rangle\}$ for $i = 1, 2, 3, 4$ and $\nu, \mu \in \{c, u, d, s\}$. The values of the mean-field parameters of SU(4) singlet and RVB_{ud} phase, in which $\{\langle \hat{F}_\mu^\nu(I_n \in A) \rangle\} = \{\langle \hat{F}_\mu^\nu(I_n \in B) \rangle\}$ is satisfied, are shown in Tables SI and SII

Table SI. Mean-field parameters $\langle \hat{F}_\mu^\nu(i) \rangle$ of SU(4) singlet phase

n	1	2	3	4	1	2	3	4	1	2	3	4	1	2	3	4
$\nu \backslash \mu$	c				u				d				s			
c	$\frac{1}{4}$	$\frac{1}{4}$	$\frac{1}{4}$	$\frac{1}{4}$	0	0	0	0	0	0	0	0	0	0	0	0
u	0	0	0	0	$\frac{1}{4}$	$\frac{1}{4}$	$\frac{1}{4}$	$\frac{1}{4}$	0	0	0	0	0	0	0	0
d	0	0	0	0	0	0	0	0	$\frac{1}{4}$	$\frac{1}{4}$	$\frac{1}{4}$	$\frac{1}{4}$	0	0	0	0
s	0	0	0	0	0	0	0	0	0	0	0	0	$\frac{1}{4}$	$\frac{1}{4}$	$\frac{1}{4}$	$\frac{1}{4}$

Table SII. Mean-field parameters $\langle \hat{F}_\mu^\nu(i) \rangle$ of RVB_{ud} phase

n	1	2	3	4	1	2	3	4	1	2	3	4	1	2	3	4
$\nu \backslash \mu$	c				u				d				s			
c	0	0	0	0	0	0	0	0	0	0	0	0	0	0	0	0
u	0	0	0	0	$\frac{1}{2}$	$\frac{1}{2}$	$\frac{1}{2}$	$\frac{1}{2}$	0	0	0	0	0	0	0	0
d	0	0	0	0	0	0	0	0	$\frac{1}{2}$	$\frac{1}{2}$	$\frac{1}{2}$	$\frac{1}{2}$	0	0	0	0
s	0	0	0	0	0	0	0	0	0	0	0	0	0	0	0	0

The singlet-RVB_{ud} solid phase is characterized by $\{\langle \hat{F}_\mu^\nu(I_n \in A) \rangle\}$ as in Table SI and $\{\langle \hat{F}_\mu^\nu(I_n \in B) \rangle\}$ as in Table SII.

2. LINEAR FLAVOR-WAVE THEORY

For convenience, we write the Hamiltonian as the sum of three terms, namely $\hat{\mathcal{H}} = \hat{\mathcal{H}}^{(J)} + \hat{\mathcal{H}}^{(J')} + \hat{\mathcal{H}}^{(D)}$, where

$$\hat{\mathcal{H}}^{(J)} = J \sum_I \sum_{\langle n, n' \rangle} \sum_{\mu, \nu} \hat{F}_\mu^\nu(I_n) \hat{F}_\nu^\mu(I_{n'}), \quad (\text{S4})$$

$$\hat{\mathcal{H}}^{(J')} = \sum_I \sum_{I'} \sum_{n, n'=1}^{N/4} \sum_{\mu, \nu}^4 \mathcal{J}'_{I_n, I'_{n'}} \hat{F}_\mu^\nu(I_n) \hat{F}_\nu^\mu(I'_{n'}), \quad (\text{S5})$$

$$\hat{\mathcal{H}}^{(D)} = D \sum_I \sum_{n=1}^{N/4} \sum_{\mu=1}^4 \left[\hat{F}_c^\mu(I_n) + \hat{F}_s^\mu(I_n) - \hat{F}_u^\mu(I_n) - \hat{F}_d^\mu(I_n) \right]. \quad (\text{S6})$$

For simplicity, here we describe in detail the next steps of the procedure for the intraplaquette hopping term $\hat{\mathcal{H}}^{(J)}$, but the same applies to the other two terms. Let \mathbf{d}_I and $\tilde{\mathbf{d}}_I$ be the column vectors whose components are the annihilation operators of the 256 original basis states of a plaquette $\{\hat{a}_{I,l}\}$ and of the PMF eigenstates, respectively:

$$\mathbf{d}_I \equiv \begin{pmatrix} \hat{a}_{I,1} \\ \hat{a}_{I,2} \\ \vdots \\ \hat{a}_{I,256} \end{pmatrix}, \quad \tilde{\mathbf{d}}_I \equiv \begin{pmatrix} \hat{g}_I \\ \hat{e}_{I,1} \\ \vdots \\ \hat{e}_{I,255} \end{pmatrix} = \begin{pmatrix} \hat{g}_I \\ \mathbf{e}_I \end{pmatrix}, \quad (\text{S7})$$

where \hat{g}_I and $\{\hat{e}_{I,m}\}$ denote the annihilation operators of the ground state and the excited states at the PMF level, respectively, and I is plaquette index. \mathbf{d}_I and $\tilde{\mathbf{d}}_I$ are related by a 256×256 unitary matrix as $\tilde{\mathbf{d}}_I = U_I \mathbf{d}_I$. We thus can represent the Hamiltonian as

$$\begin{aligned} \hat{\mathcal{H}}^{(J)} &= J \sum_I \sum_{\langle n, n' \rangle} \sum_{\mu, \nu} \mathbf{d}_I^\dagger \hat{F}_\mu^\nu(I_n) \hat{F}_\nu^\mu(I_{n'}) \mathbf{d}_I \\ &= J \sum_I \sum_{\langle n, n' \rangle} \sum_{\mu, \nu} \tilde{\mathbf{d}}_I^\dagger U_I \hat{F}_\mu^\nu(I_n) \hat{F}_\nu^\mu(I_{n'}) U_I^\dagger \tilde{\mathbf{d}}_I. \end{aligned} \quad (\text{S8})$$

The matrix $\sum_{\langle n, n' \rangle} \sum_{\mu, \nu} U_I \hat{F}_\mu^\nu(I_n) \hat{F}_\nu^\mu(I_{n'}) U_I^\dagger$ has block form:

$$\sum_{\langle n, n' \rangle} \sum_{\mu, \nu} U_I \hat{F}_\mu^\nu(I_n) \hat{F}_\nu^\mu(I_{n'}) U_I^\dagger = \begin{pmatrix} \alpha_I^{(J)} & \mathbf{u}_I^{(J)\top} \\ \mathbf{v}_I^{(J)} & \mathcal{A}_I^{(J)} \end{pmatrix} \begin{matrix} \updownarrow 1 \\ \updownarrow 255 \end{matrix} \begin{matrix} \leftarrow 1 \rightarrow \\ \leftarrow 255 \rightarrow \end{matrix}$$

From this we obtain

$$\hat{\mathcal{H}}^{(J)} = J \left(\sum_{I \in \text{A}}^{N/8} + \sum_{I \in \text{B}}^{N/8} \right) \left[\alpha_I^{(J)} \hat{g}_I^\dagger \hat{g}_I + \hat{g}_I^\dagger \mathbf{u}_I^{(J)\top} \cdot \mathbf{e}_I + \mathbf{e}_I^\dagger \cdot \mathbf{v}_I^{(J)} \hat{g}_I + \mathbf{e}_I^\dagger \mathcal{A}_I^{(J)} \mathbf{e}_I \right]. \quad (\text{S9})$$

\hat{g}_I and $\{\hat{e}_{I,m}\}$ obey the bosonic commutation relations under the constraint

$$\hat{g}_I^\dagger \hat{g}_I + \sum_m \hat{e}_{I,m}^\dagger \hat{e}_{I,m} = \hat{g}_I^\dagger \hat{g}_I + \mathbf{e}_I^\dagger \cdot \mathbf{e}_I = 1. \quad (\text{S10})$$

Following the analogy with the spin-wave expansion method, we may expand the Hamiltonian with

$$\hat{g}_I^\dagger = \sqrt{1 - \mathbf{e}_I^\dagger \cdot \mathbf{e}_I} \simeq 1 - \frac{1}{2} \mathbf{e}_I^\dagger \cdot \mathbf{e}_I + \dots, \quad (\text{S11})$$

under the assumption that the fluctuations $\mathbf{e}_I^\dagger \cdot \mathbf{e}_I$ around the PMF ground state are sufficiently small. The Hamiltonian becomes

$$\hat{\mathcal{H}}^{(J)} = E_0^{(J)} + \hat{\mathcal{H}}_1^{(J)} + \hat{\mathcal{H}}_2^{(J)} + \hat{\mathcal{H}}_3^{(J)} + \dots, \quad (\text{S12})$$

where

$$E_0^{(J)} = \alpha_I^{(J)} \quad (\text{S13})$$

$$\hat{\mathcal{H}}_1^{(J)} = \mathbf{u}_I^{(J)\top} \cdot \mathbf{e}_I + \mathbf{e}_I^\dagger \cdot \mathbf{v}_I^{(J)} \quad (\text{S14})$$

$$\hat{\mathcal{H}}_2^{(J)} = -\alpha_I^{(J)} \mathbf{e}_I^\dagger \cdot \mathbf{e}_I + \mathbf{e}_I^\dagger \mathcal{A}_I^{(J)} \mathbf{e}_I \quad (\text{S15})$$

$$\hat{\mathcal{H}}_3^{(J)} = -\frac{1}{2} \left(\mathbf{e}_I^\dagger \cdot \mathbf{e}_I \mathbf{u}_I^{(J)\top} \cdot \mathbf{e}_I + \mathbf{e}_I^\dagger \cdot \mathbf{v}_I^{(J)} \mathbf{e}_I^\dagger \cdot \mathbf{e}_I \right) \quad (\text{S16})$$

Note that $\hat{\mathcal{H}}_1^{(J)} = 0$ is justified when we consider the full Hamiltonian. Following the assumption of the plaquette-checkerboard structure (A-plaquette and B-plaquette), we define the following Fourier transformation

$$\mathbf{e}_{I \in \text{A}} = \frac{1}{\sqrt{N/8}} \sum_{\mathbf{k} \in \text{B.Z.}} \mathbf{e}_{\mathbf{k}}^{(\text{A})} \exp(i\mathbf{k} \cdot \mathbf{r}_{I \in \text{A}}) \quad (\text{S17})$$

$$\mathbf{e}_{I \in B} = \frac{1}{\sqrt{N/8}} \sum_{\mathbf{k} \in B.Z.} \mathbf{e}_{\mathbf{k}}^{(B)} \exp(i\mathbf{k} \cdot \mathbf{r}_{I \in B}) \quad (\text{S18})$$

where \mathbf{r}_I is the position vector of the center of the plaquette I . We obtain

$$\begin{aligned} E_0^{(J)} + \hat{\mathcal{H}}_2^{(J)} &= J \sum_{\mathbf{k}} \left[-\alpha_{I \in A}^{(J)} \mathbf{e}_{\mathbf{k}}^{(A)\dagger} \cdot \mathbf{e}_{\mathbf{k}}^{(A)} + \mathbf{e}_{\mathbf{k}}^{(A)\dagger} \mathcal{A}_{I \in A}^{(J)} \mathbf{e}_{\mathbf{k}}^{(A)} \right. \\ &\quad \left. -\alpha_{I \in B}^{(J)} \mathbf{e}_{\mathbf{k}}^{(B)\dagger} \cdot \mathbf{e}_{\mathbf{k}}^{(B)} + \mathbf{e}_{\mathbf{k}}^{(B)\dagger} \mathcal{A}_{I \in B}^{(J)} \mathbf{e}_{\mathbf{k}}^{(B)} \right] + \frac{1}{8} J N (\alpha_{I \in A}^{(J)} + \alpha_{I \in B}^{(J)}). \end{aligned} \quad (\text{S19})$$

Applying the same procedure to the other terms we arrive at

$$\begin{aligned} E_0^{(D)} + \hat{\mathcal{H}}_2^{(D)} &= J \sum_{\mathbf{k}} \left[-\alpha_{I \in A}^{(D)} \mathbf{e}_{\mathbf{k}}^{(A)\dagger} \cdot \mathbf{e}_{\mathbf{k}}^{(A)} + \mathbf{e}_{\mathbf{k}}^{(A)\dagger} \mathcal{A}_{I \in A}^{(D)} \mathbf{e}_{\mathbf{k}}^{(A)} \right. \\ &\quad \left. -\alpha_{I \in B}^{(D)} \mathbf{e}_{\mathbf{k}}^{(B)\dagger} \cdot \mathbf{e}_{\mathbf{k}}^{(B)} + \mathbf{e}_{\mathbf{k}}^{(B)\dagger} \mathcal{A}_{I \in B}^{(D)} \mathbf{e}_{\mathbf{k}}^{(B)} \right] + \frac{1}{8} D N (\alpha_{I \in A}^{(D)} + \alpha_{I \in B}^{(D)}), \end{aligned} \quad (\text{S20})$$

$$\begin{aligned} E_0^{(J')} + \hat{\mathcal{H}}_2^{(J')} &= \sum_{I \in A}^{N/8} \sum_{n, n'=1}^4 \sum_{\mu, \nu} \sum_{\mathbf{k}} \frac{1}{2} \mathcal{J}'_{I_n, I'_{n'}} \left[-\alpha_{I_n}^{(J')\nu} \alpha_{I'_{n'}}^{(J')\mu} \mathbf{e}_{\mathbf{k}}^{(B)\dagger} \cdot \mathbf{e}_{\mathbf{k}}^{(B)} + \alpha_{I_n}^{(J')\nu} \mathbf{e}_{\mathbf{k}}^{(B)\dagger} \mathcal{A}_{I'_{n'}}^{(J')\mu} \mathbf{e}_{\mathbf{k}}^{(B)} \right] + \\ &\quad \sum_{I' \in B}^{N/8} \sum_{n, n'=1}^4 \sum_{\mu, \nu} \sum_{\mathbf{k}} \left[\frac{1}{2} \mathcal{J}'_{I_n, I'_{n'}} \left(-\alpha_{I_n}^{(J')\nu} \alpha_{I'_{n'}}^{(J')\mu} \mathbf{e}_{\mathbf{k}}^{(A)\dagger} \cdot \mathbf{e}_{\mathbf{k}}^{(A)} + \alpha_{I'_{n'}}^{(J')\mu} \mathbf{e}_{\mathbf{k}}^{(A)\dagger} \mathcal{A}_{I_n}^{(J')\nu} \mathbf{e}_{\mathbf{k}}^{(A)} \right) \right. \\ &\quad \left. + 2\gamma_{-\mathbf{k}, I_n, I'_{n'}} \left\{ \mathbf{e}_{\mathbf{k}}^{(A)\top} \left(\mathbf{u}_{I_n}^{(J')\nu} \otimes \mathbf{u}_{I'_{n'}}^{(J')\mu\top} \right) \mathbf{e}_{-\mathbf{k}}^{(B)} + \mathbf{e}_{\mathbf{k}}^{(A)\top} \left(\mathbf{u}_{I_n}^{(J')\nu} \otimes \mathbf{v}_{I'_{n'}}^{(J')\mu\top} \right) \mathbf{e}_{\mathbf{k}}^{(B)*} \right\} \right. \\ &\quad \left. + 2\gamma_{\mathbf{k}, I_n, I'_{n'}} \left\{ \mathbf{e}_{\mathbf{k}}^{(A)\dagger} \left(\mathbf{v}_{I_n}^{(J')\nu} \otimes \mathbf{u}_{I'_{n'}}^{(J')\mu\top} \right) \mathbf{e}_{\mathbf{k}}^{(B)} + \mathbf{e}_{\mathbf{k}}^{(A)\dagger} \left(\mathbf{v}_{I_n}^{(J')\nu} \otimes \mathbf{v}_{I'_{n'}}^{(J')\mu\top} \right) \mathbf{e}_{-\mathbf{k}}^{(B)*} \right\} \right] \\ &\quad + \sum_{I \in A}^{N/8} \sum_{I' \in B}^{N/8} \sum_{n, n'=1}^4 \sum_{\mu, \nu} \frac{1}{2} \mathcal{J}'_{I_n, I'_{n'}} \alpha_{I_n}^{(J')\nu} \alpha_{I'_{n'}}^{(J')\mu} + (A \leftrightarrow B), \end{aligned} \quad (\text{S21})$$

where

$$\gamma_{\mathbf{k}, I_n, I'_{n'}} = \frac{1}{4} \mathcal{J}'_{I_n, I'_{n'}} \exp[i(\mathbf{r}_{I'} - \mathbf{r}_I) \cdot \mathbf{k}]. \quad (\text{S22})$$

Passing to the Bogoliubov matrix representation of the full Hamiltonian we get

$$\hat{\mathcal{H}} = \frac{1}{2} \sum_{\mathbf{k}} \begin{pmatrix} \mathbf{e}_{\mathbf{k}}^{(A)\dagger} & \mathbf{e}_{\mathbf{k}}^{(B)\dagger} & \mathbf{e}_{-\mathbf{k}}^{(A)\top} & \mathbf{e}_{-\mathbf{k}}^{(B)\top} \end{pmatrix} H_{\mathbf{k}} \begin{pmatrix} \mathbf{e}_{\mathbf{k}}^{(A)} \\ \mathbf{e}_{\mathbf{k}}^{(B)} \\ \mathbf{e}_{-\mathbf{k}}^{(A)*} \\ \mathbf{e}_{-\mathbf{k}}^{(B)*} \end{pmatrix} + E_0 - \frac{1}{2} \sum_{\mathbf{k}} \text{Tr} A_{-\mathbf{k}}^*, \quad (\text{S23})$$

where $H_{\mathbf{k}}$ is the 1020×1020 Hermitian matrix made up of four square blocks:

$$H_{\mathbf{k}} = \begin{pmatrix} A_{\mathbf{k}} & B_{\mathbf{k}} \\ B_{-\mathbf{k}}^* & A_{-\mathbf{k}}^* \end{pmatrix}, \quad (\text{S24})$$

$$A_{\mathbf{k}} = \begin{pmatrix} (-J\alpha_{I_A}^{(J)} - D\alpha_{I_A}^{(D)})\mathbb{1} + J\mathcal{A}_{I_A}^{(J)} + D\mathcal{A}_{I_A}^{(D)} & \mathbb{O} \\ \mathbb{O} & (-J\alpha_{I_B}^{(J)} - D\alpha_{I_B}^{(D)})\mathbb{1} + J\mathcal{A}_{I_B}^{(J)} + D\mathcal{A}_{I_B}^{(D)} \end{pmatrix} + \sum_{\mu,\nu} \sum_{n,n'=1}^4 \left[\sum_{I' \in B}^{N/8} \begin{pmatrix} \Gamma_1 + \Gamma_2 & \Gamma_4 \\ \mathbb{O} & \mathbb{O} \end{pmatrix} + \sum_{I' \in A}^{N/8} \begin{pmatrix} \mathbb{O} & \mathbb{O} \\ \mathbb{O} & \Gamma_1 + \Gamma_3 \end{pmatrix} + \sum_{I' \in A}^{N/8} \begin{pmatrix} \mathbb{O} & \mathbb{O} \\ \Gamma_4 & \mathbb{O} \end{pmatrix} \right] \quad (S25)$$

$$B_{\mathbf{k}} = \sum_{\mu,\nu} \sum_{n,n'=1}^4 \left[\sum_{I' \in B}^{N/8} \begin{pmatrix} \mathbb{O} & \Gamma_5 \\ \mathbb{O} & \mathbb{O} \end{pmatrix} + \sum_{I' \in A}^{N/8} \begin{pmatrix} \mathbb{O} & \mathbb{O} \\ \Gamma_5 & \mathbb{O} \end{pmatrix} \right] \quad (S26)$$

$$\begin{cases} \Gamma_1 = -\mathcal{J}'_{I_n, I'_{n'}} \alpha_{I_n}^{(J')\nu} \alpha_{I'_{n'}}^{(J')\mu} \mathbb{1} \\ \Gamma_2 = \mathcal{J}'_{I_n, I'_{n'}} \alpha_{I'_{n'}}^{(J')\mu} \mathcal{A}_{I_n}^{(J')\nu} \\ \Gamma_3 = \mathcal{J}'_{I_n, I'_{n'}} \alpha_{I_n}^{(J')\mu} \mathcal{A}_{I'_{n'}}^{(J')\nu} \\ \Gamma_4 = 4\gamma_{\mathbf{k}, I_n, I'_{n'}} \left(\mathbf{v}_{I_n}^{(J')\nu} \otimes \mathbf{u}_{I'_{n'}}^{(J')\mu\top} \right) \\ \Gamma_5 = 4\gamma_{\mathbf{k}, I_n, I'_{n'}} \left(\mathbf{v}_{I_n}^{(J')\nu} \otimes \mathbf{v}_{I'_{n'}}^{(J')\mu\top} \right) \end{cases} \quad (S27)$$

Here, $\mathbb{1}$ and \mathbb{O} are the 255×255 identity matrix and zero matrix, respectively. $H_{\mathbf{k}}$ is diagonalized by a Bogoliubov transformation

$$\begin{pmatrix} \mathbf{e}_{\mathbf{k}}^{(A)} \\ \mathbf{e}_{\mathbf{k}}^{(B)} \\ \mathbf{e}_{-\mathbf{k}}^{(A)*} \\ \mathbf{e}_{-\mathbf{k}}^{(B)*} \end{pmatrix} = U_{\mathbf{k}}^P \begin{pmatrix} \hat{\varepsilon}_{\mathbf{k},1} \\ \vdots \\ \hat{\varepsilon}_{\mathbf{k},510} \\ \hat{\varepsilon}_{-\mathbf{k},1}^\dagger \\ \vdots \\ \hat{\varepsilon}_{-\mathbf{k},510}^\dagger \end{pmatrix} \quad (S28)$$

where $U_{\mathbf{k}}^P$ is the 1020×1020 paraunitary matrix. We obtain the diagonalized form as

$$\hat{\mathcal{H}}_2 = \sum_{\mathbf{k}} \sum_{\lambda=1}^{510} \omega_{\mathbf{k},\lambda} \hat{\varepsilon}_{\mathbf{k},\lambda}^\dagger \hat{\varepsilon}_{\mathbf{k},\lambda} + E_{\text{zp}}, \quad (S29)$$

where $\omega_{\mathbf{k},\lambda}$ is the λ -th excitation energy band and

$$E_{\text{zp}} = \frac{1}{2} \sum_{\mathbf{k}} \sum_{\lambda} \omega_{\mathbf{k},\lambda} - \frac{1}{2} \sum_{\mathbf{k}} \text{Tr} A_{-\mathbf{k}}^*. \quad (S30)$$

3. FURTHER COMMENTS ON THE VALIDITY OF THE LFWT APPROACH

In the main text we pointed out that our LFWT approach is more reliable in the regime of small J'/J because it is based on the PMF approximation. Here we discuss another aspect, namely the validity of the expansion of the square root in Eq. 4 in the main text and the subsequent truncation that leads to the Bogoliubov Hamiltonian. Such procedure can be justified only when the occupation of the excited states $\langle \mathbf{e}_I^\dagger \cdot \mathbf{e}_I \rangle = \sum_n \langle \hat{e}_{I,n}^\dagger \hat{e}_{I,n} \rangle$ is small. In Fig. S1 we show various constant- $\langle \mathbf{e}_I^\dagger \cdot \mathbf{e}_I \rangle$ lines within the different phases in the phase diagram. For the states with a two-sublattice structure, we picked the larger one from $\langle \mathbf{e}_I^\dagger \cdot \mathbf{e}_I \rangle$ for $I \in A$ and $I \in B$. As can be seen this quantity is independent of D (within our approximations) except for jumps at phase boundaries and, most importantly, it is sufficiently small in a large region of the phase diagram; in particular it does not exceed 0.1 for $J'/J < 0.4$. This analysis provides an *a posteriori* justification of the LFWT treatment, especially in the region of the parameter space where also the assumptions of the PMF approximation are more under control. The AFM phase has a relatively higher value of $\langle \mathbf{e}_I^\dagger \cdot \mathbf{e}_I \rangle$, which is of course expected and related to the well-known magnetic moment depletion of quantum antiferromagnets.

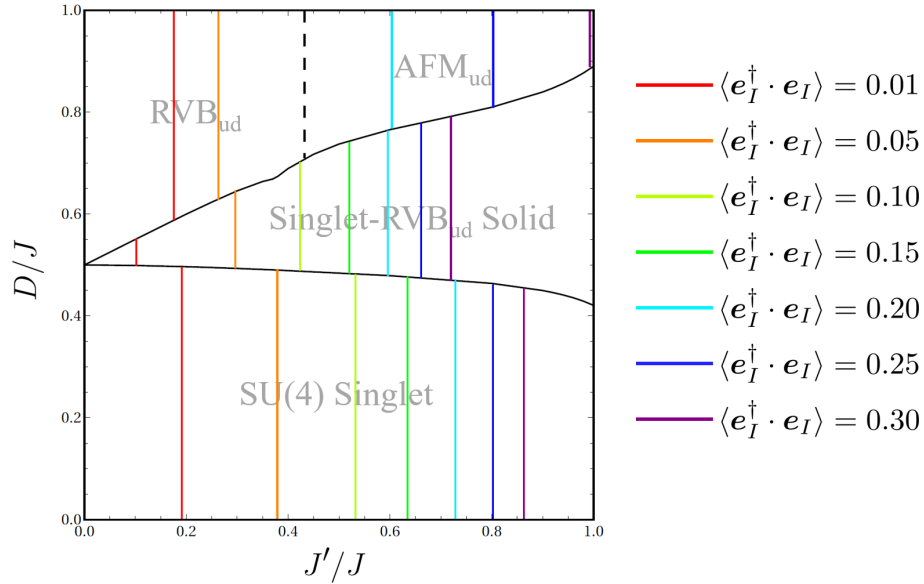


Fig. S1. Constant- $\langle \mathbf{e}_I^\dagger \cdot \mathbf{e}_I \rangle$ lines within the various phases.